Acta Oceanol. Sin., 2024, Vol. 43, No. 5, P. 91–99
https://doi.org/10.1007/s13131-024-2321-z
http://www.aosocean.com
E-mail: ocean2@hyxb.org.cn

Simulating the evolution of focused waves by a two-layer Boussinesq-type model

Ping Wang[1], Zhongbo Liu[2*], Kezhao Fang[3], Wenfeng Zou[3], Xiangke Dong[1], Jiawen Sun[1]

[1] State Environmental Protection Key Laboratory of Marine Ecosystem Restoration, National Marine Environmental Monitoring Center, Dalian 116023, China

[2] College of Transportation Engineering, Dalian Maritime University, Dalian 116026, China

[3] State Key Laboratory of Coastal and Offshore Engineering, Dalian University of Technology, Dalian 116024, China

Received 30 July 2023; accepted 3 January 2024

Abstract

Accurate simulation of the evolution of freak waves by the wave phase focusing method requires accurate linear and nonlinear properties, especially in deep-water conditions. In this paper, we analyze the ability to simulate deep-water focused waves of a two-layer Boussinesq-type (BT) model, which has been shown to have excellent linear and nonlinear performance. To further improve the numerical accuracy and stability, the internal wave-generated method is introduced into the two-layer Boussinesq-type model. Firstly, the sensitivity of the numerical results to the grid resolution is analyzed to verify the convergence of the model; secondly, the focused wave propagating in two opposite directions is simulated to prove the symmetry of the numerical results and the feasibility of the internal wave-generated method; thirdly, the limiting focused wave condition is simulated to compare and analyze the wave surface and the horizontal velocity of the profile at the focusing position, which is in good agreement with the measured values. Meanwhile the simulation of focused waves in very deep waters agrees well with the measured values, which further demonstrates the capability of the two-layer BT model in simulating focused waves in deep waters.

Key words: focused waves, numerical simulation, Boussinesq-type model, velocity profile

Citation: Wang Ping, Liu Zhongbo, Fang Kezhao, Zou Wenfeng, Dong Xiangke, Sun Jiawen. 2024. Simulating the evolution of focused waves by a two-layer Boussinesq-type model. Acta Oceanologica Sinica, 43(5): 91–99, doi: 10.1007/s13131-024-2321-z

1 Introduction

Large waves, known as freak or rogue waves, have been of great concern over the last 30 years because of their potential to destroy a passing ship or man-made structures at sea. Evidence shows that freak waves can occur in deep water, finite depth water or shallow water. Many issues such as the generation, propagation and transformation of freak waves or the interaction between freak waves and floating structures become hot. Many efforts have been made to understand the behavior of such large wave events (Kharif and Pelinovsky, 2003), the physical mechanics for the generation of freak waves are phase focusing, non-linear wave-wave interaction such as modulation instability, the effect of adverse currents, the effect of bottom friction or even the effect of wind.

The observation of large wave event such as "New Year" waves (Haver and Andersen, 2000) usually happens at a fixed location, but the researchers were only able to obtain some basic behaviors, mainly due to the harsh ocean conditions at the site, which prevented detailed measurements of extreme large waves. To obtain more detailed information on freak waves, many physical experiments have been carried out, such as focused wave group evolution in a flume or basin (Baldock et al., 1996; Baldock and Swan, 1996; Johannessen and Swan, 2001; Liu and Hong, 2004; Ma et al., 2010). In contrast to the laboratory studies, accurate numerical simulation of focused waves is becoming feasible and popular, and therefore many efforts have been devoted to the development of various numerical models, such as higher-order boundary element model (HOBEM) (Ning et al., 2008, 2009), higher-order spectral (HOS) method based on potential flow theory (Zhao et al., 2009; Ducrozet et al., 2012; Li and Liu, 2015), one-layer Boussinesq-type (BT) model (Fuhrman and Madsen, 2010) and multi-layer Boussinesq-type models (Liu and Fang, 2016; Liu et al., 2019), high-level Green-Naghdi models and harmonic polynomial cell (HPC) method (Zhao et al., 2020), a general boundary-fitted 3D non-hydrostatic model (Ai et al., 2014), and a constrained interpolation profile (CIP) model with an internal wave maker (Li et al., 2018). These studies showed that freak waves can be obtained by the wave phase focusing method, and the accurate simulation of the surface wave height and its velocity profiles under the focused wave crest could not be obtained by the linear Stokes wave theory, the second-order Stokes wave theory, or the stream wave theory, because the freak waves are local high-nonlinear wave events with different spectra.

The Boussinesq-type models, which are widely used in ocean wave simulation, have many advantages in terms of computational efficiency and nonlinear wave interactions. There are many sophisticated versions of BT models (Madsen et al., 1991; Nwogu, 1993; Wei et al., 1995). Due to the inaccuracy of the third-order nonlinear properties including amplitude dispersion, these BT models with Padé [2, 2] or Padé [4, 4] dispersion could not accurately describe the evolution of highly nonlinear wave events such as freak waves, especially at deep-water conditions. As far as

Foundation item: The National Natural Science Foundation under contract Nos 52171247, 51779022, 52071057, and 51709054.
*Corresponding author, E-mail: liuzhongbo@dlmu.edu.cn

we know, there are only two types of BT models that can accurately simulate focused waves with strong nonlinearities in deep water, including one-layer BT model (Madsen et al., 2002) and multi-layer BT models (Liu and Fang, 2016), which have been verified to have accurate dispersion and nonlinear properties in modelling extreme waves. Recently, numerical results have validated the fundamental ability of multi-layer BT models in modelling highly nonlinear wave cases (Liu et al., 2018, 2019; Liu and Fang, 2019), the evolution of free surface waves generated by bottom motion (Fang et al., 2020), and highly nonlinear solitary propagation and transformation over complex bathymetries (Fang et al., 2022).

In the evolution of the focused wave, high accuracy in both linear and nonlinear properties is required in numerical models. Firstly, phase-focused waves contain a variety of frequencies, and high-precision linear dispersion is a basic requirement for accurate modelling the wave focusing process. Secondly, wave-wave interactions generate high harmonics, so the second-order nonlinear characteristics of the model are also important. Thirdly, for extreme waves, the third-order characteristics play an obvious role in the highly nonlinear occurrence of waves in a short period of time, and fourthly, the simulation accuracy of the vertical velocity is also particularly important for the focused wave, which requires high accuracy of the BT model in the vertical direction. Due to the inaccuracy of linear and nonlinear characteristics, the traditional BT model cannot accurately simulate the focused waves in deep water, which is the reason why there is very little literature on the simulation of freak waves using BT models.

The aim of the present paper is to investigate and study the capability of a two-layer BT model (Liu and Fang, 2016) in modelling the evolution of focused waves. To solve the possible negative effect in wave generation due to the third-order terms included in the model, an internal wave-generated method proposed by Hsiao et al. (2005) is used in the present model with sponge layer absorption on both sides of the numerical flume. The numerical models are presented in Section 2, validation and discussion are given in Section 3, and final conclusions are given in Section 4.

2 Numerical model

2.1 *Governing equations*

Liu and Fang (2016) developed a new two-layer BT model under the Cartesian coordinate system. In the derivation, the main assumptions include a homogeneous fluid with constant density, incompressibility and irrationality of the flow, and the absence of viscous and surface tension effects.

The total water depth is divided into two layers, see in Fig. 1, η is the surface elevation, h_1 is the thickness of the upper water column, z_1 is the middle of the upper water column, h_2 is the thickness of the lower water column, z_2 is the middle of the lower water column. The authors used two sets of computational velocity components (u_1, w_1) defined at $z = z_1$ in the upper layer and (u_2, w_2) defined at $z = z_2$ in the lower layer. Then the velocity profiles in each layer can be obtained by using the Taylor expansion method. To further improve the accuracy of the equation, (u_1, w_1) and (u_2, w_2) can be expressed by the pseudo velocities (u_1*, w_1*) and (u_2*, w_2*) in Eqs (1)–(4), which will achieve a much higher order accuracy without increasing the order of the derivatives by introducing Padé approximants in the truncated equations.

$$u_1 \equiv {u_1}^* + \frac{1}{10}{z_1}^2\nabla(\nabla\cdot{u_1}^*), \tag{1}$$

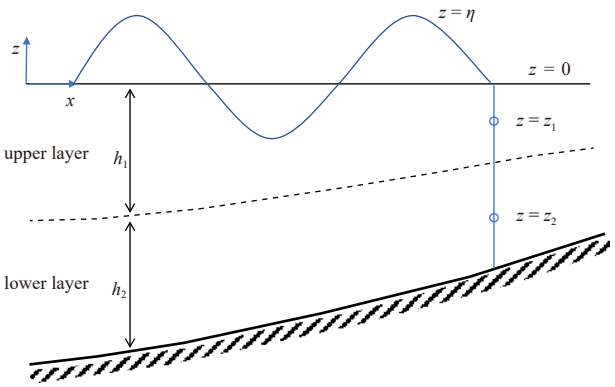

Fig. 1. Wave propagates over mildly sloping topographies.

$$w_1 \equiv {w_1}^* + \frac{1}{10}{z_1}^2\nabla\cdot(\nabla{w_1}^*), \tag{2}$$

$$u_2 \equiv {u_2}^* + \frac{1}{10}(z_2+h_1)^2\nabla(\nabla\cdot{u_2}^*), \tag{3}$$

$$w_2 \equiv {w_2}^* + \frac{1}{10}(z_2+h_1)^2\nabla\cdot(\nabla{w_2}^*). \tag{4}$$

The resulting two-layer BT model embodies high accuracy in linear phase velocity, second-order and third-order nonlinear properties, linear shoaling properties and kinematic properties from extremely deep to shallow water (Liu and Fang, 2016). Specifically, the model is applicable to up to $kh \approx 53$ in linear phase velocity, up to $kh \approx 30$ in the second-order nonlinear property including super harmonics and subharmonics within 1% error, and up to $0 < kh < 60$ in the linear shoaling property within 0.13% tolerance error, where k is the wave number and h is the water depth. The accuracy of velocity profiles can also be applicable to up to $kh \approx 22.4$ within 1% error. Further details such as the derivation and the theoretical analysis can be referred to Liu and Fang (2016).

The vertical two-dimensional version of the two-layer BT model (Liu and Fang, 2016) consists of nine independent variables: the surface elevation η, the pseudo velocities (u_1*, w_1*) and (u_2*, w_2*) on the middle of each water column layer ($z = z_1$ and $z = z_2$), the velocities (u_η, w_η) on the free surface ($z = \eta$). and the velocities (u_{10}, w_{10}) on the still water level ($z = 0$). The equations of the two-layer BT model consist of the following nine equations.

(1) The kinematic and dynamic free surface conditions can be written as

$$\frac{\partial\eta}{\partial t} = w_\eta - u_\eta\eta_x, \tag{5}$$

$$\frac{\partial u_\eta}{\partial t} = -g\eta_x - \frac{1}{2}\left({u_\eta}^2 + 2u_\eta w_\eta\eta_x\right)_x - \eta_x\frac{\partial w_\eta}{\partial t} + w_\eta\left(u_\eta\eta_x\right)_x. \tag{6}$$

(2) The group of velocity (u_η, w_η) on the free surface is obtained by using Taylor expansion to velocities (u_{10}, w_{10}), and they are written as

$$u_\eta = u_{10} + \eta w_{10x} - \frac{1}{2}\eta^2 u_{10xx} - \frac{1}{6}\eta^3 w_{10xxx}, \tag{7}$$

$$w_\eta = w_{10} - \eta u_{10x} - \frac{1}{2}\eta^2 w_{10xx} + \frac{1}{6}\eta^3 u_{10xxx}. \tag{8}$$

(3) The formulas for the velocity components (u_{10}, w_{10}) on still water level can be obtained according to the following formulas:

$$u_{10} = u_1^* - \sigma_1 u_{1xx}^* + \sigma_2 w_{1x}^* - \sigma_3 w_{1xxx}^* - \sigma_4 u_{1x}^* + \sigma_5 u_{1xxx}^* - \sigma_6 w_{1xx}^*, \tag{9}$$

$$w_{10} = w_1^* - \sigma_1 w_{1xx}^* - \sigma_2 u_{1x}^* + \sigma_3 u_{1xxx}^* - \sigma_4 w_{1x}^* + \sigma_5 w_{1xxx}^* + \sigma_6 u_{1xx}^*. \tag{10}$$

(4) The velocity matching conditions at the interface between the two layers satisfy the conditions are as follows:

$$u_2^* - \sigma_7 u_{2xx}^* + \sigma_8 w_{2x}^* - \sigma_9 w_{2xxx}^* - \sigma_{10} u_{2x}^* + \sigma_{11} u_{2xxx}^* (1 - c_1) - \sigma_{12} \left(1 - \frac{1}{4} c_1\right) w_{2xx}^* = u_1^* - \sigma_1 u_{1xx}^* - \sigma_2 w_{1x}^* + \sigma_3 w_{1xxx}^* + 3\sigma_4 u_{1x}^* - \sigma_5 u_{1xxx}^* - \frac{3}{2}\sigma_6 w_{1xx}^*, \tag{11}$$

$$w_2^* - \sigma_7 w_{2xx}^* - \sigma_8 u_{2x}^* + \sigma_9 u_{2xxx}^* - \sigma_{10} w_{2x}^* + \sigma_{11}(1 - c_1) w_{2xxx}^* + \sigma_{12} \left(1 - \frac{1}{4} c_1\right) u_{2xx}^* = w_1^* - \sigma_1 w_{1xx}^* + \sigma_2 u_{1x}^* - \sigma_3 u_{1xxx}^* + \sigma_4 w_{1x}^* - 3\beta_{13}\sigma_5 w_{1xxx}^* + \frac{3}{2}\beta_{12}\sigma_6 u_{1xx}^*. \tag{12}$$

(5) The kinematic condition at the bottom is written as

$$w_2^* - \sigma_7 w_{2xx}^* + \sigma_8 u_{2x}^* - \sigma_9 u_{2xxx}^* + \sigma_{10} w_{2x}^* - 3\beta_{23}\sigma_{11} \left(1 + \frac{1}{3} c_1\right) w_{2xxx}^* + \frac{3}{2}\beta_{22}\sigma_{12} \left(1 + \frac{1}{6} c_1\right) u_{2xx}^* + h_x (u_2^* - \sigma_7 u_{2xx}^* - \sigma_8 w_{2x}^* + \sigma_9 w_{2xxx}^*) = 0. \tag{13}$$

In the above equations, the subscript x denotes the first order partial derivative with respect to x, and the subscript xx denotes the second order partial derivative, the subscript xxx denotes the third order partial derivative. g is the acceleration of gravity. In present paper, the coefficients (α_1, α_2, β_{12}, β_{13}, β_{22}, β_{23}) = (0.105 3, 0.394 7, 0.920, 0.850, 0.937, 0.607) are utilized, the coefficient $c_1 = -\frac{2\alpha_1}{2\alpha_1 + \alpha_2}$, and the formulations for σ_i (i = 1, 2, ..., 12) are as follows:

$$\begin{cases} \sigma_2 = \alpha_1 h, \\ \sigma_8 = \alpha_2 h, \\ \sigma_1 = \frac{2}{5}\sigma_2^2, \\ \sigma_7 = \frac{2}{5}\sigma_8^2, \\ \sigma_3 = \frac{1}{15}\sigma_2^3, \\ \sigma_9 = \frac{1}{15}\sigma_8^3, \\ \sigma_4 = \alpha_1^2 h h_x, \\ \sigma_5 = \frac{1}{5}\alpha_1^4 h^3 h_x, \\ \sigma_6 = \frac{4}{5}\alpha_1^3 h^2 h_x, \\ \sigma_{10} = (2\alpha_1 + \alpha_2)\sigma_8 h_x, \\ \sigma_{11} = \frac{1}{5}\sigma_8^2 \sigma_{10}, \\ \sigma_{12} = \frac{4}{5}\sigma_8 \sigma_{10}. \end{cases} \tag{14}$$

2.2 *Numerical scheme*

The highest derivative in the equations is limited to three, which is similar to the BT model proposed by Wei et al. (1995), and these spatial derivatives do not present any difficulties in numerical discretization. And the numerical method proposed in the FUNWAVE model is widely used to solve traditional BT models in the literature, and we also follow this approach to solve our model. A composite fourth-order Adams-Bashforth-Moulton integration scheme is used for time marching. A predictor-corrector-iteration step is employed to solve the model. The steps in the predictor stage are listed as follows:

(1) Calculate the predicted values of η and u_η via Eqs (5) and (6) by using the variables defined at the current time step on the right-hand side of the equations.

(2) Calculate the predicted value of u_{10} by substituting the predicted values of η and u_η from Step (n) into Eq. (7) and using the variable w_{10} at the current time level.

(3) Using the predicted values and repeating the same procedure as in Step (n + 1), u_1* can be obtained from Eq. (9) and u_2* from Eq. (11).

(4) Substituting all predicted values into the right-hand side of Eq. (13), the vertical velocity w_2* defined at the lower layer can be obtained.

(5) Calculate w_1* using Eq. (12), w_{10} using Eq. (10) and w_η using Eq. (8) using the available predicted values used.

In the corrector stage, the similar process is iterated until the error of the nine variables between the two iterations reaches a predetermined value, such as 0.000 1. And the convergence of the iterations is accelerated by using an over-relaxation technique proposed by Kirby et al. (1998).

The centered finite difference method is used to calculate the spatial derivatives of the inner grid, and the one-sided difference scheme is used at the boundary points. For unknown velocity variables, the second-order finite difference scheme is used to approximate their first-order and second-order spatial derivatives, while the third-order derivatives are shifted to the right-hand side of the equations and evaluated by using the current time-level quantities. This produces a tri-diagonal matrix which is efficiently solved by using the Thomas algorithm. The remaining first-order and second-order spatial derivatives for the known quantities on the right-hand side of the equations are approximated using a fourth-order finite difference scheme. Note that all the third-order spatial derivatives are discretized to second-order accuracy.

In calculation of η and u_η values at time Step (n + 1), the third-order Adams-Bashforth time scheme is used for the prediction step, and the fourth-order Adams-Moulton scheme is used for the correction step, which is as

$$\eta^{n+1} - \eta^n = \frac{\Delta t}{12}(23F^n - 16F^{n-1} + 5F^{n-2}), \tag{15}$$

$$\eta^{n+1} - \eta^n = \frac{\Delta t}{24}(9F^{n+1} + 19F^n - 5F^{n-1} + F^{n-2}), \tag{16}$$

where the superscript n denotes the time step corresponding to the parameter value at time $n \times \Delta t$, and n + 1 corresponds to the parameter value at time $(n + 1) \times \Delta t$, F represents the remaining terms in Eqs (5) and (6) except time derivative term.

2.3 *An internal wave maker in numerical model*

The BT model usually uses the boundary wave generation method, but the reflection due to the change of water depth can

make the numerical results unreliable; at the same time, the numerical results can be affected by the incident boundary conditions when solving the third-order derivatives using the one-sided difference scheme at the boundary points; the internal wave generation method (Wei et al., 1999; Chawla and Kirby, 2000) can avoid the above problems and have better stability compared with the boundary wave generation methods. The internal wave generation methods that work for Boussinesq-type models with Padé [2, 2] or Padé [4, 4] dispersion (Wei et al., 1999; Gobbi and Kirby, 1999) cannot be used in the model provided by Liu et al. (2018, 2019), whose dispersion relation equation is Padé [6, 8]. Therefore, the present model employs the internal wave generation method proposed by Hsiao et al. (2005) to simulate the focusing waves, and uses a sponge layer for the absorption on the sides of the numerical flume. The source expression of the Internal wave-generated method is written as follows:

$$\xi = K\frac{\Delta t}{T}\frac{C_g}{C}\frac{H}{2}\exp[-\beta(x-x_0)^2]\cos(kx-\omega t)\,. \tag{17}$$

where K is the coefficient of wave generation method, according to Hsiao et al. (2005), a value of $K = 8.28$ is recommended to achieve more accurate and stable wave processes in a two-dimensional numerical wave tank; Δt is the time step in numerical model; T is the incident wave period; C_g is the wave group velocity; C is the wave speed; $\beta = 20/L^2$; L is the wavelength; k is the wave number; (x, y) are the coordinates of the grid points, x_0 are the coordinates of the wave generation source points; ω is the wave angular frequency; t is the running time in numerical model. The width of the internal wave generation method in the numerical model is one wavelength, and ξ is the increment of the wave surface elevation at each step.

3 Numerical validations and discussions

3.1 *The convergence of spatial steps to numerical results*

Before verifying of the numerical model, the convergence of spatial steps to the numerical results is considered. The water depth is 0.7 m, and the frequencies proposed by Baldock et al. (1996) are used with Cases B50 and D50, where 50 means that a value of 50 mm is used for the linear focusing amplitude A_f. In Case B50, 29 different wave components are set with wave periods ranging from 0.6 s to 1.4 s, where the interval ΔT between two consecutive individual wave period is a constant, i.e., ΔT = 0.8/28 s, and the wave amplitude of each portion is 50/29 mm. In Case D50, the wave periods range from 0.8 s to 1.2 s. In the numerical simulations, the computational domain is 24 m in length with the center line of the internal wave maker is positioned 6m from the left side of the flume, and a 4 m long sponge layer is placed at both ends of the numerical flume. In both cases, the linear theoretical focusing position is x = 8 m at the focusing time t_f = 30 s. Three spatial steps dx = 0.02 m, 0.04 m, and 0.06 m with the time step dt = 0.01 s are used in the simulations.

The surface elevation at locations x = 2 m, 4 m, 6 m, and 8 m are compared to validate the convergence of the spatial step. The numerical results for Cases B50 and D50 are shown in Figs 2 and 3, respectively. From these two figures, we can clearly see that the small difference occurs at the wave crest, and with the decrease of the spatial step, the results are slightly higher at the wave crest and they are much closer to a stable stage. The numerical results are almost identical, which indicates that the spatial convergence is observed. In addition, the convergence of the time step is also verified and is not presented here for brevity.

3.2 *The symmetry of the numerical model*

To check the symmetry of a numerical model, Case D55 (Baldock et al., 1996) is re-run using the numerical models. The length of the numerical flume is 30 m, the centerline of the wave maker is positioned 15 m from the left side of the flume. The time step used in the simulation is 0.01 s and the spatial step is 0.03 m. The numerical results of the positions x = 2 m, 4 m, 6 m, and 8 m to the right of the wave maker and the symmetrical positions to the left are analyzed. The computed surface elevation (right from

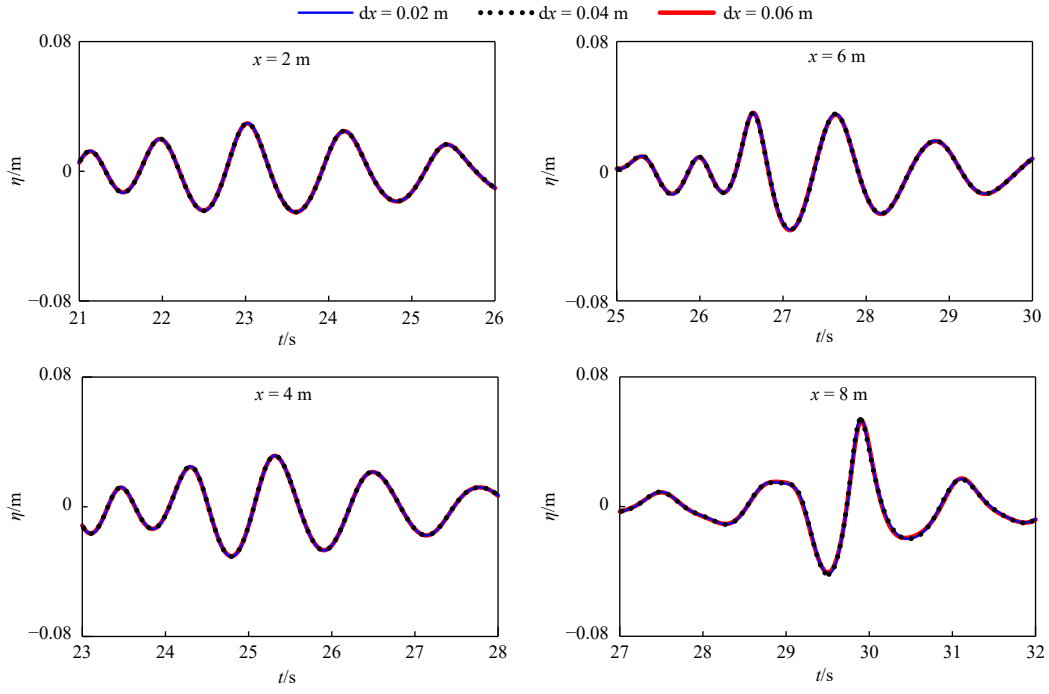

Fig. 2. Time history of surface elevation at different locations for Case B50.

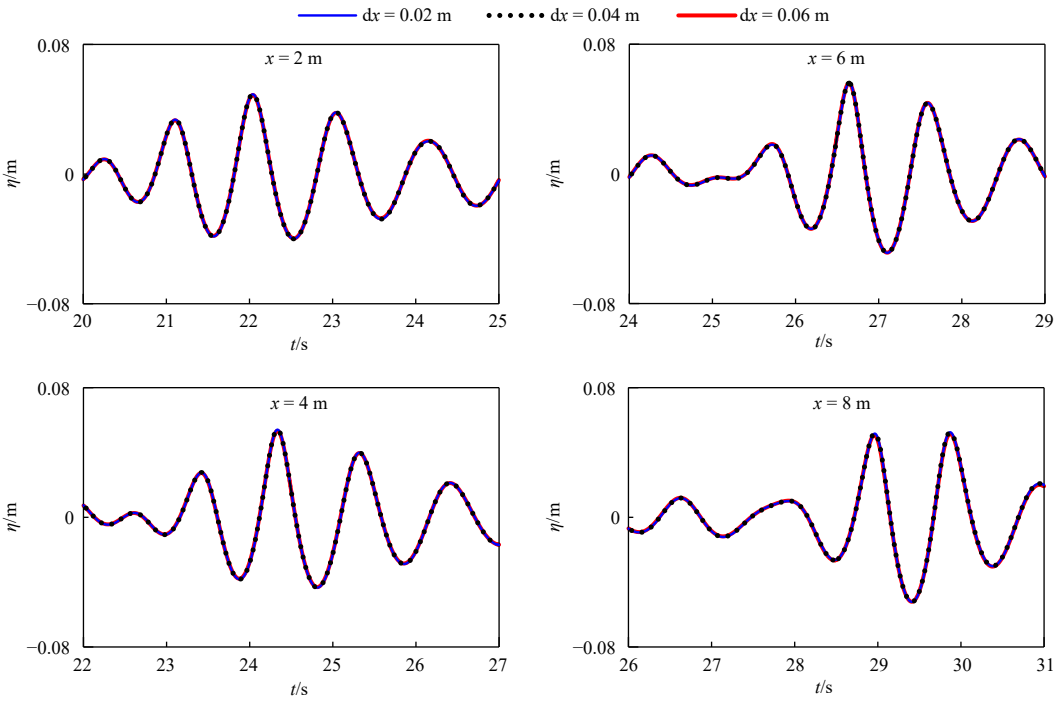

Fig. 3. Time history of surface elevation at different locations for Case D50.

centerline of the wave maker) is compared with those from left (left from centerline of the wave maker), as shown in Fig. 4, and the two numerical results are almost identical, which shows a perfect symmetry of the two-layer BT model.

3.3 *The comparisons with the experimental measurements in Baldock et al. (1996)*

Baldock et al. (1996) carried out a series of wave experiments at the Department of Civil Engineering, Imperial College (UK) to investigate the spatio-temporal focusing of a wide range of uni-directional waves on deep water. The incident wave group consists of several wave components. It is essential that the motion of each component and their interactions are accurately traced. Cases B22, B38, B55, D22, D38, and D55 from the experiments are used to validate the present the two-layer BT model. The wave groups consist of $N = 29$ individual wave components with equal wave amplitude, and the narrow frequency band covers the range of kh within 2.026–4.403 (Cases D22, D38, and D55) and the wider frequency band covers the range of kh within 1.57–7.83 (Cases B22, B38, and B55) over a constant water depth of 0.7 m.

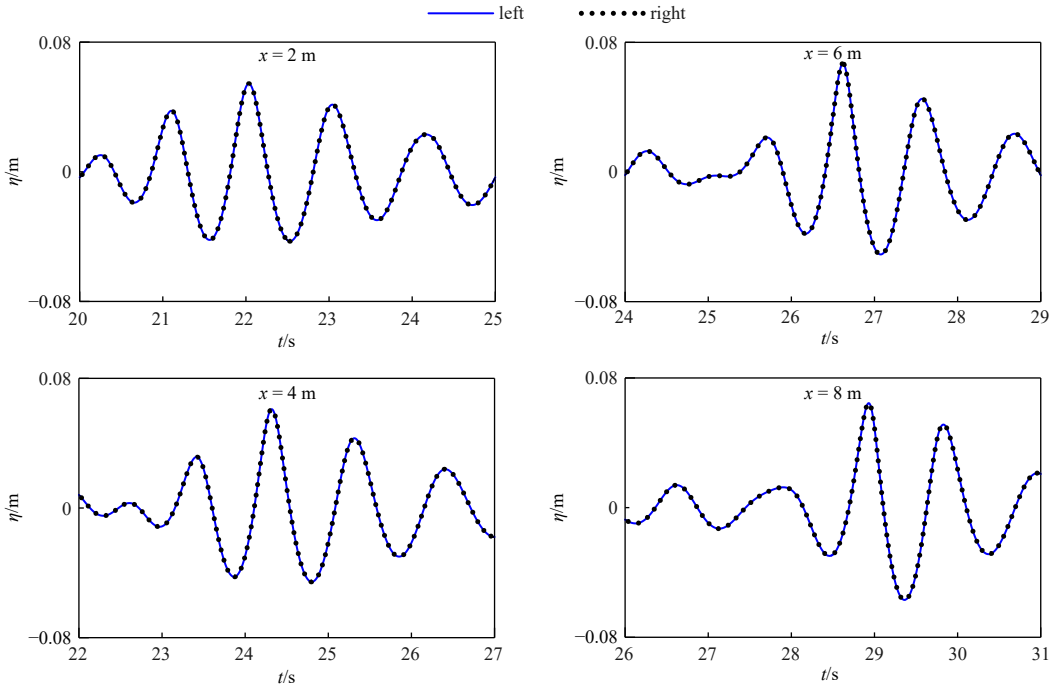

Fig. 4. Time history of surface elevation at different locations for Case D55.

The total computational length is 20 m, and the centerline of the internal wave maker is positioned 6 m from the left side of the flume, and a 4 m long sponge layer is applied at both ends of the computational domain. The spatial and temporal steps are 0.02 m and 0.01 s, respectively.

The comparisons of the computed focused waves from the present two-layer model with the experimental data are shown in Fig. 5, and the wave evolution at four locations x_1 (x_1 stands for the distance before the focused location) is compared with experimental measurements and the numerical results of Smith and Swan (2002), where the numerical simulations were carried out with a potential flow model, as shown in Fig. 6. Good agreements are found between the numerical calculations and the experimental measurements. Meanwhile, we note that our numerical results are also in good agreement with the numerical results of Smith and Swan (2002). The corresponding vertical horizontal profiles under the wave crest are plotted in Fig. 7. Again, to facilitate the comparisons, the numerical results on Case B55 and Case D55 from Smith and Swan (2002) are also digital in this figure. Overall, the agreement is good.

To explain why the present two-layer BT model shows a higher focused wave crest, some reasons are listed below. Firstly, the tests carried out in the experimental flume have a certain attenuation in wave height due to the viscosity dissipation or the effect of the side wall during the wave propagation. Secondly, the waves generated by the boundary wave maker are slightly different from those generated by the linear internal wave maker. Thirdly, the experimental flume cannot overcome the reflection from the boundary, and the reflected waves may "contaminate" the experimental measurements.

3.4 *comparisons with the numerical results from Zhao et al. (2020)*

Numerical simulations of focused waves in extremely deep water have been performed by Zhao et al. (2020). Different from Cases B and D of Baldock et al. (1996), the water depth in the study of Zhao et al. (2020) simulation is set to h = 2.1 m, and the actual focused wave crests η_f in numerical simulations are η_f = 55 mm or 22 mm, respectively. Thus, the narrow frequency band covers the range of kh within 4.31–23.48 (Cases B_3) and the wider frequency band covers the range of kh within 5.57–13.21 (Cases D_3) over a constant water depth of 2.1 m. Since the nonlinearity in Cases $B_3\eta_f22$ and $D_3\eta_f22$ is too weak, we choose Cases $B_3\eta_f55$ and $D_3\eta_f55$ to validate our numerical model, the time step is 0.01 s and spatial step is 0.02 m in numerical model. The numerical results are compared with those of Zhao et al. (2020), who

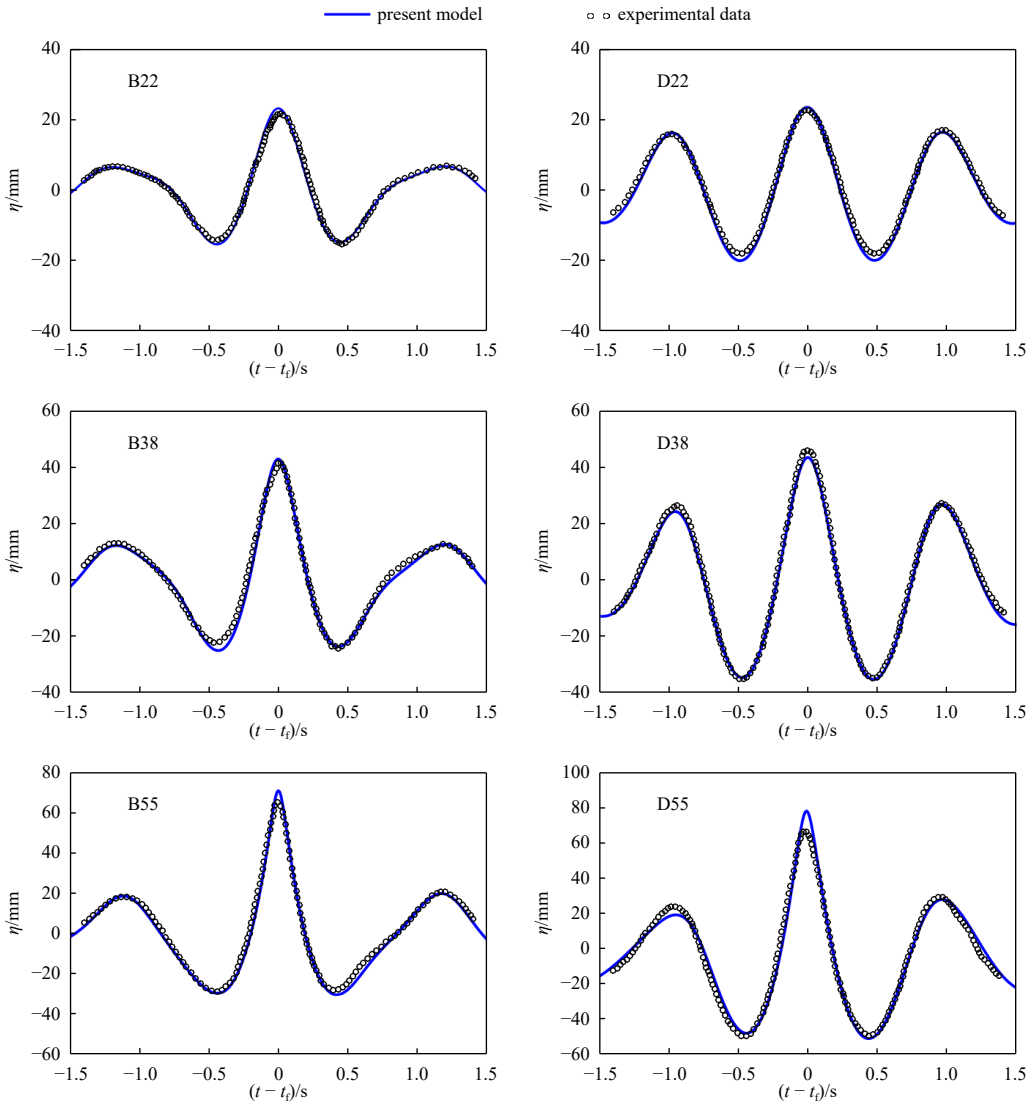

Fig. 5. Comparison of the calculated focused wave elevation with the experimental results of Baldock et al. (1996).

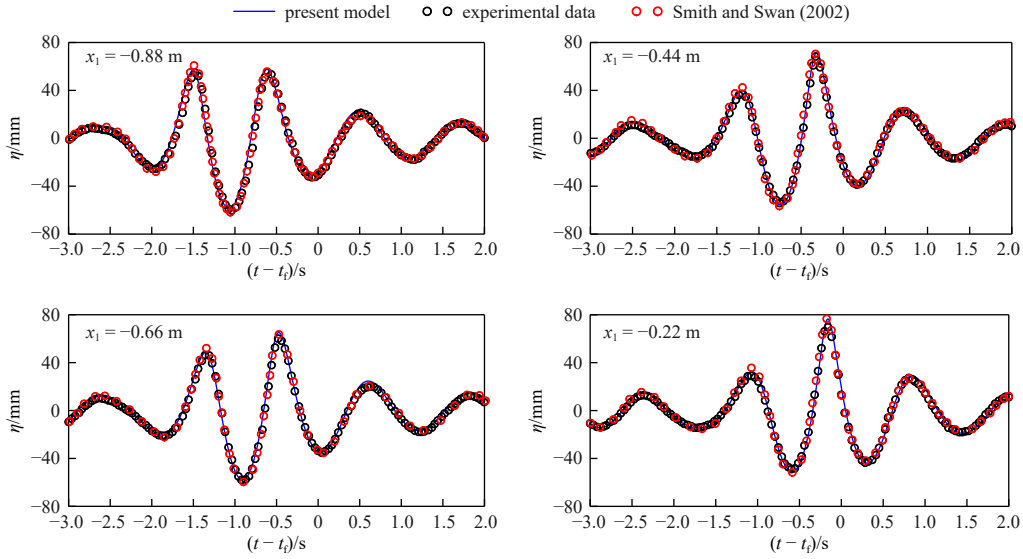

Fig. 6. Comparisons between the calculated wave elevation at four locations and the experimental results of Baldock et al. (1996)

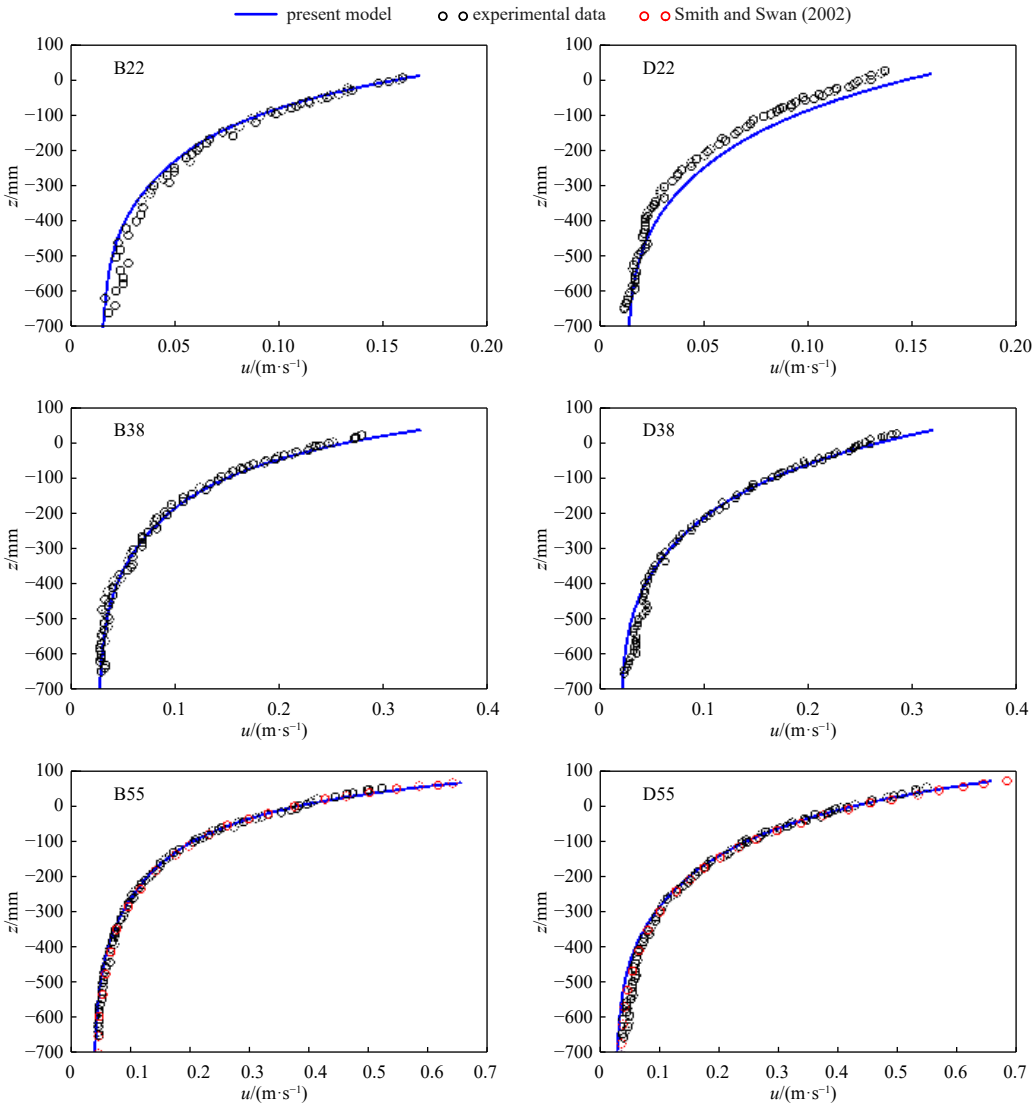

Fig. 7. Comparisons of velocity profiles between modeled and experimental data of Baldock et al. (1996).

use the high-level Green-Naghdi models to simulate these two cases. To obtain η_f = 55 mm in our numerical simulations, the linearly focused wave crest A_f is 46 mm and 43.3 mm for $B_3\eta_f55$ and $D_3\eta_f55$, respectively, which is 46 mm and 42 mm in Zhao et al. (2020). The calculated focused surface elevations and horizontal velocity profiles beneath the focused wave crest are shown in Figs 8 and 9. The two numerical results are similar to each other, which partly demonstrates the high accuracy of our model. In order to accurately describe the velocity profile, more layers are needed, and the three-layer or four-layer BT models (Liu et al., 2018, 2019) are essential, which will be investigated in the future.

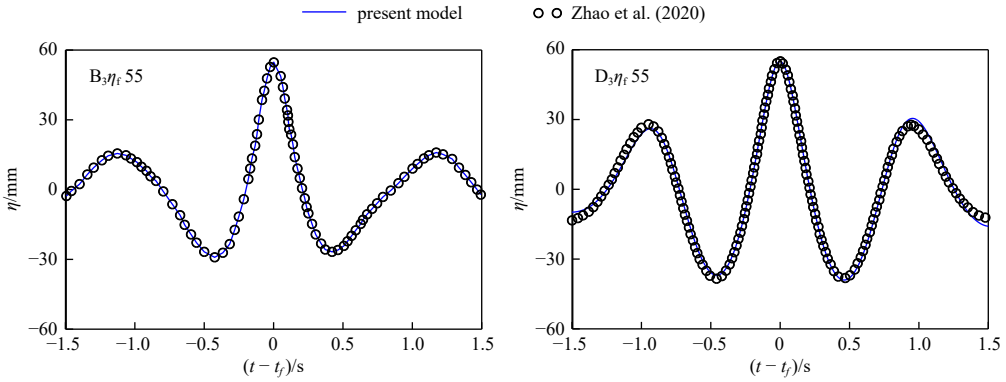

Fig. 8. The comparisons of the focused crest.

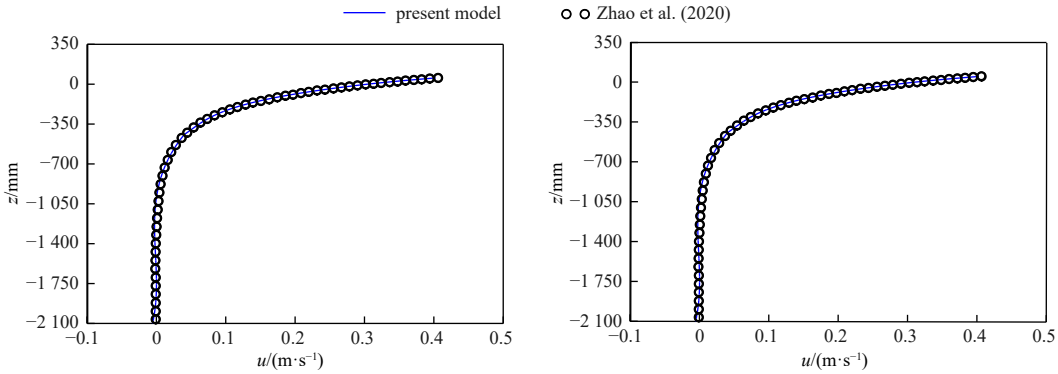

Fig. 9. Horizontal velocity beneath the focused crest.

4 Conclusions

The two-layer BT numerical model in this paper has demonstrated high accuracy in both linear and nonlinear characteristics, and the internal wave-generated method is introduced into the two-layer BT model to simulate the extreme focusing wave conditions. Numerical experiments are carried out for wave generation, propagation, and evolution under different water depth conditions, the following conclusions are drawn from this study.

(1) The numerical convergence of the two-layer BT model is very good, and the numerical results of the focused wave along the middle of the flume to the two sides have a perfect symmetry, which demonstrates the internal wave-generated method provided by Hsiao et al. (2005) is applicable to the two-layer BT model in this paper, and it can be used to simulate the limiting focused wave conditions with high nonlinearity and dispersion requirements.

(2) Several focused wave conditions from the experiments (Baldock et al., 1996) are simulated. The simulated wavefronts at the focusing position and the horizontal profile velocities under the focusing peaks are in good agreement with the experimental results, indicating that the two-layer BT model can simulate complex wave evolutions due to the highly nonlinearity of the local wave peaks, especially in the representation of the vertical velocities of the waves.

(3) The focused wave under deep water conditions with the frequency band of kh within 4.31–23.48 are simulated. The comparison between the numerical model and the experiment demonstrates that the two-layer BT model also have high accuracy in both linear and nonlinear properties for extremely deep-water conditions. Three or more layers of BT models need to be developed to accurately describe the velocity profile under more extreme water depth conditions.

References

Ai Congfang, Ding Weiye, Jin Sheng. 2014. A general boundary-fitted 3D non-hydrostatic model for nonlinear focusing wave groups. Ocean Engineering, 89: 134–145, doi: 10.1016/j.oceaneng.2014.08.002

Baldock T E, Swan C. 1996. Extreme waves in shallow and intermediate water depths. Coastal Engineering, 27(1/2): 21–46, doi: 10.1016/0378-3839(95)00040-2

Baldock T E, Swan C, Taylor P H. 1996. A laboratory study of nonlinear surface waves on water. Philosophical Transactions of the Royal Society of London. Series A: Mathematical, Physical and Engineering Sciences, 354(1707): 649–676

Chawla A, Kirby J T. 2000. A source function method for generation of waves on currents in Boussinesq models. Applied Ocean Research, 22(2): 75–83, doi: 10.1016/S0141-1187(00)00005-5

Ducrozet G, Bonnefoy F, Le Touzé D, et al. 2012. A modified high-order spectral method for wavemaker modeling in a numerical

wave tank. European Journal of Mechanics-B/Fluids, 34: 19–34, doi: 10.1016/j.euromechflu.2012.01.017

Fang Kezhao, Liu Zhongbo, Sun Jiawen, et al. 2020. Development and validation of a two-layer Boussinesq model for simulating free surface waves generated by bottom motion. Applied Ocean Research, 94: 101977, doi: 10.1016/j.apor.2019.101977

Fang Kezhao, Liu Zhongbo, Wang Ping, et al. 2022. Modeling solitary wave propagation and transformation over complex bathymetries using a two-layer Boussinesq model. Ocean Engineering, 265: 112549, doi: 10.1016/j.oceaneng.2022.112549

Fuhrman D R, Madsen P A. 2010. Numerical simulation of extreme events from focused directionally spread wavefields. In: Coastal Engineering-30th International Conference. San Diego, CA, USA: World Scientific, 772–781

Gobbi M F, Kirby J T. 1999. Wave evolution over submerged sills: Tests of a high-order Boussinesq model. Coastal Engineering, 37(1): 57–96, doi: 10.1016/S0378-3839(99)00015-0

Haver S, Andersen O J. 2000. Freak waves: Rare realizations of a typical population or typical realizations of a rare population?. In: Proceedings of the 10th International Offshore and Polar Engineering Conference. Seattle, WA, USA: ISOPE,123–130

Hsiao S C, Lynett P, Hwung H H, et al. 2005. Numerical simulations of nonlinear short waves using a multilayer model. Journal of Engineering Mechanics, 131(3): 231–243, doi: 10.1061/(ASCE)0733-9399(2005)131:3(231)

Johannessen T B, Swan C. 2001. A laboratory study of the focusing of transient and directionally spread surface water waves. Proceedings of the Institution of Mechanical Engineers, Part M: Journal of Engineering for the Maritime Environment, 457(2008): 971–1006

Kharif C, Pelinovsky E. 2003. Physical mechanisms of the rogue wave phenomenon. European Journal of Mechanics-B/Fluids, 22(6): 603–634, doi: 10.1016/j.euromechflu.2003.09.002

Kirby J T, Wei G, Chen Qin, et al. 1998. FUNWAVE 1.0: Fully nonlinear Boussinesq wave model-documentation and user's manual. Research Report No. CACR-98–06. NewarkDE, USA: University of Delaware

Li Jinxuan, Liu Shuxue. 2015. Focused wave properties based on a high order spectral method with a non-periodic boundary. China Ocean Engineering, 29(1): 1–16, doi: 10.1007/s13344-015-0001-7

Li Mengyu, Zhao Xizeng, Ye Zhouteng, et al. 2018. Generation of regular and focused waves by using an internal wave maker in a CIP-based model. Ocean Engineering, 167: 334–347, doi: 10.1016/j.oceaneng.2018.08.048

Liu Shuxue, Hong Qiying. 2004. The generation method of three-dimensional focusing wave and its properties. Haiyang Xuebao (in Chinese), 26(6): 133–142

Liu Zhongbo, Fang Kezhao. 2016. A new two-layer Boussinesq model for coastal waves from deep to shallow water: Derivation and Analysis. Wave Motion, 67: 1–14, doi: 10.1016/j.wavemoti.2016.07.002

Liu Zhongbo, Fang Kezhao. 2019. Numerical verification of a two-layer Boussinesq-type model for surface gravity wave evolution. Wave Motion, 85: 98–113, doi: 10.1016/j.wavemoti.2018.11.007

Liu Zhongbo, Fang Kezhao, Cheng Y Z. 2018. A new multi-layer irrotational Boussinesq-type model for highly nonlinear and dispersive surface waves over a mildly sloping seabed. Journal of Fluid Mechanics, 842: 323–353, doi: 10.1017/jfm.2018.99

Liu Zhongbo, Fang Kezhao, Sun Jiawen. 2019. A multi-layer Boussinesq-type model with second-order spatial derivatives: Theoretical analysis and numerical implementation. Ocean Engineering, 191: 106545, doi: 10.1016/j.oceaneng.2019.106545

Ma Yuxiang, Dong Guohai, Liu Shuxue, et al. 2010. Laboratory study of unidirectional focusing waves in intermediate depth water. Journal of Engineering Mechanics, 136(1): 78–90, doi: 10.1061/(ASCE)EM.1943-7889.0000076

Madsen P A, Bingham H B, Liu Hua. 2002. A new Boussinesq method for fully nonlinear waves from shallow to deep water. Journal of Fluid Mechanics, 462: 1–30, doi: 10.1017/S0022112002008467

Madsen P A, Murray R, Sørensen O R. 1991. A new form of the Boussinesq equations with improved linear dispersion characteristics. Coastal Engineering, 15(4): 371–388, doi: 10.1016/0378-3839(91)90017-B

Ning Dezhi, Teng Bin, Eatock Taylor R, et al. 2008. Numerical simulation of non-linear regular and focused waves in an infinite water-depth. Ocean Engineering, 35(8/9): 887–899, doi: 10.1016/j.oceaneng.2008.01.015

Ning Dezhi, Zang Jun, Liu Shuxue, et al. 2009. Free-surface evolution and wave kinematics for nonlinear uni-directional focused wave groups. Ocean Engineering, 36(15/16): 1226–1243, doi: 10.1016/j.oceaneng.2009.07.011

Nwogu O. 1993. Alternative form of Boussinesq equations for nearshore wave propagation. Journal of Waterway, Port, Coastal, and Ocean Engineering, 119(6): 618–638

Smith S F, Swan C. 2002. Extreme two-dimensional water waves: an assessment of potential design solutions. Ocean Engineering, 29(4): 387–416, doi: 10.1016/S0029-8018(01)00028-2

Wei Ge, Kirby J T, Grilli S T, et al. 1995. A fully nonlinear Boussinesq model for surface waves. Part 1. Highly nonlinear unsteady waves. Journal of Fluid Mechanics, 294: 71–92, doi: 10.1017/S0022112095002813

Wei Ge, Kirby J T, Sinha A. 1999. Generation of waves in Boussinesq models using a source function method. Coastal Engineering, 36(4): 271–299, doi: 10.1016/S0378-3839(99)00009-5

Zhao Xizeng, Sun Zhaochen, Liang Shuxiu. 2009. Efficient focusing models for generation of freak waves. China Ocean Engineering, 23(3): 429–440

Zhao Binbin, Zheng Kun, Duan Wenyang, et al. 2020. Time domain simulation of focused waves by high-level irrotational Green-Naghdi equations and harmonic polynomial cell method. European Journal of Mechanics-B/Fluids, 82: 83–92, doi: 10.1016/j.euromechflu.2020.02.006